Archaeometry **62**, 2 (2020) 247–266 doi: 10.1111/arcm.12517

CHEMICAL AND MINERALOGICAL CHARACTERIZATION OF AGUADA PORTEZUELO POTTERY FROM CATAMARCA, NORTH-WESTERN ARGENTINA: PIXE, XRD AND SEM-EDS STUDIES APPLIED TO SURFACE PRE- AND POST-FIRING PAINTS, SLIPS AND PASTES*

G. A. DE LA FUENTE†
Laboratorio de Petrología y Conservación Cerámica, Escuela de Arqueología, Universidad Nacional de Catamarca—CITCa., CONICET, 4700 Catamarca Argentina

V. G. JOSA, G. CASTELLANO, S. LIMANDRI
Instituto de Física Enrique Gaviola, CONICET—Universidad Nacional de Córdoba, Córdoba Argentina

S. D. VERA
Laboratorio de Petrología y Conservación Cerámica, Escuela de Arqueología, Universidad Nacional de Catamarca—CITCa., CONICET, 4700 Catamarca Argentina

J. F. DÍAS
Instituto de Física, Universidade Federal do Río Grande do Sul (UFRGS), Río Grande do Sul, Brazil

S. SUÁREZ and G. BERNARDI
Centro Atómico Bariloche (CAB), Comisión Nacional de Energía Atómica, Av. E. Bustillo 9500, San Carlos de BarilocheR8402AGP, Argentina

and S. BERTOLINO
Instituto de Física Enrique Gaviola, CONICET—Universidad Nacional de Córdoba, Córdoba Argentina

Particle-induced X-ray emission (PIXE), X-ray diffraction (XRD), electron microprobe analysis (EDS) and scanning electron microscopy (SEM) analytical techniques were used to characterize surface paints in pre- and post-fired Aguada Portezuelo decorated pottery. Surface paintings in black, white, red, brown, burgundy and ochre were analysed. Major, minor and trace elements were detected by PIXE, whereas XRD and SEM-EDS gave information on the main mineral phases and the characteristic morphology for each analysed pigment. The results obtained indicate that the main colour groups can be easily discriminated by PIXE, and they are characterized by only one pigment for each colour: hematite (red) and manganese mineral oxides (black), respectively, whereas white pigments are characterized by calcite, ghelenite and gypsum.

KEYWORDS: PIXEXRDSEM-EDSAGUADA PORTEZUELOMIDDLE PERIODNORTH-WESTERN ARGENTINA

---

*Received 12 March 2019; accepted 25 October 2019
†Corresponding author: email gfuente2004@yahoo.com.ar

INTRODUCTION

Archaeological materials such as ceramics are examples of inhomogeneous systems at the micrometric scale. Their surface characteristics depend on their conservation state, which is related to the weathering suffered by the pieces. In general, the information related to their composition and manufacturing processes are not completely known. In this sense, chemical and crystallographic characterization techniques may provide valuable information. Nevertheless, the correct characterization of these materials is a challenge since standard destructive characterization procedures cannot be usually applied, due to the fact that keeping the material unaltered is a priority in cultural heritage samples.

From its beginning in the 1970s, ion beam analysis (IBA) techniques have been successfully applied to study historical and cultural objects; and since the 1990s they have been systematically used for material analysis (e.g., Ruvalcaba-Sil and Demortier 1997; Neelmeijer *et al.* 2000; Olsson *et al.* 2001; Ruvalcaba-Sil 2005; Hall 2006; Rizzuto *et al.* 2007, 2014; Rivero-Torres *et al.* 2008; Abd El Aal *et al.* 2009; Grassi *et al.* 2009; Poupeau *et al.* 2010; Lima *et al.* 2011; Gajić-Kvaščev *et al.* 2012; Ikeoka *et al.* 2013; Šmit *et al.* 2013; Calligaro *et al.* 2015; Pappalardo *et al.* 2015, 2016; Santos *et al.* 2015; Dasari *et al.* 2017). Nowadays, the advances in the characterization methodologies are centred in their application to areas with specific limitations, such as archaeometry. For an excellent review of particle-induced X-ray emission (PIXE) applications in archaeological ceramics, see Rizzuto and Tabacniks (2017). Although the chemical state and crystallographic structure of compounds cannot be studied by IBA techniques, they allow the determination of elemental compositions with detection limits as low as a few ppm. In addition, the thickness and composition of different layers forming the piece, as well as depth concentration profiles, can be obtained by these techniques (Ruvalcaba-Sil *et al.* 1999). This information, along with mineralogical data provided by X-ray diffraction (XRD), allow archaeologists to address archaeometric questions regarding the provenance of the pieces, raw materials used, and the technology used in their production (De La Fuente *et al.* 2005; De La Fuente and Pérez Martínez 2008, 2018; Bertolino *et al.* 2009; Galván Josa *et al.* 2010; Roumié *et al.* 2010). Several limitations have to be taken into account for the proper interpretation of the results, since many archaeological objects, particularly ceramic pieces, have been buried for over 1000 years, suffered weathering and partial removal of the paints, so the paint layer thickness is not homogeneous and the surfaces are rough (De La Fuente *et al.* 2005; Bertolino *et al.* 2009; Galván Josa *et al.* 2009, 2010).

This paper presents the analytical results obtained by combining PIXE, XRD and scanning electron microscopy-electron microprobe analysis (SEM-EDS) techniques for the characterization of the archaeological paintings, slips and pastes of Aguada Portezuelo pottery belonging to the Middle period of the Catamarca Valley (*c*.600–900 CE) in the province of Catamarca, north-western Argentina. PIXE concentrations on major, minor and trace elements for different colour groups are further discussed. Chemical and mineralogical information is integrated to obtain a broad picture of the technological processes involved in the decoration of these vessels.

Aguada Portezuelo ceramic style

The Aguada Culture is one of the most spectacular of north-western Argentina because of its iconographic complexity (also called the ‘draconian style’) and high technical skill apparent in its pottery. According to different studies, this culture emerged as a consequence of a social and ideological change that occurred in the fourth to 12th centuries CE in the Ambato Valley, and progressively spread out regionally to other geographical areas such as the Hualfín and

Catamarca valleys, and northern La Rioja (Pérez Gollán 1991; González 1998, Baldini *et al.* 2002, Laguens 2007, Pantorrilla and Núñez Regueiro 2006).

The Aguada Portezuelo ceramic style (*c*.600–900), typical of the Catamarca Valley, presents a great variation and complexity in the manufacturing techniques employed by the ancient potters, particularly the surface treatments and other decoration applied to the ceramic vessels (Kusch 1996–97; González 1998; De La Fuente *et al.* 2005; De La Fuente and Pérez Martínez 2008, 2018; Nazar and De La Fuente 2016). Ceramic vessels have a complex technical elaboration process involving at least two different firing steps during which several pigments were used by ancient potters as chromophores to obtain different coloured pre- and post-firing paintings (Nazar and De La Fuente 2016). One of the highlight characteristics of these ceramics is their marked polychromy: the motifs are a complex use of negative and positive space, and the colours used range from purple red, reddish, black and yellow; the latter colour is unique in the archaeological ceramics from north-western Argentine (González 1998; De La Fuente and Pérez Martínez 2008, 2018, 3, fig. 1a; Nazar and De La Fuente 2016, 167, fig. 12). Sometimes, the colours have not been very well fixed by the firing and they appear as faint and dull, presenting pre- and post-firing paintings (Nazar and De La Fuente 2016, 166–172; De La Fuente and Pérez Martínez 2018, 6). Another of the technical decorative aspects rarely studied for this ceramic type is the use of resistant negative paintings (González 1998). Additionally, a manufacturing attribute of particular importance is the surface treatment. The internal surface of the vessels has sometimes an intense polished black colour; in others it is burnished, perhaps involving a technical process of smoking the internal surface of the vessels, also so-called ‘graffited’ (De La Fuente and Pérez Martínez 2008, 2018, 13; Nazar and De La Fuente 2016, 168–171). For an extensive description and classification of the Aguada Portezuelo ceramic style, see De La Fuente and Pérez Martínez (2008, 2018) and Nazar and De La Fuente (2016).

Pre- and post-firing paintings of this pottery have been extensively analysed by Raman microspectroscopy, and less intensively by XRD and SEM-EDS. The results of this previous research indicate that red and ochre are characterized exclusively by hematite pigment ($\alpha\text{-}Fe_2O_3$); black presents a more variable composition, with manganese (Mn) oxide minerals (pirolusite ($Mn^{+4}O_2$) and psilomelane ($BaMn^{+2} + Mn_8O_{16}\ (OH)_4$)) predominantly responsible for this colour; magnetite (Fe_3O_4) (sometimes titane-magnetite) is also present. A white colour (a pre-firing slip) is the most variable compound, resulting from calcite (CO_3Ca), gypsum ($CaSO_4.2H_2O$) and gehlenite ($Ca_2\ [Al_2(SiO_2)]$) mineral phases, although titanium oxide (TiO_2) and hydroxyapatite ($Ca_{10}\ [PO_4]6\ [OH]_2$) have also been identified (Cremonte *et al.* 2003; De La Fuente *et al.* 2005; De La Fuente and Pérez Martínez 2008, 2018; Bertolino *et al.* 2009; Galván Josa *et al.* 2009, 2010).

SAMPLING

Pottery sherd samples were chosen from a collection as being representative or unique in their technological classes. Different samples were considered, all corresponding to the Aguada Portezuelo ceramic style, as described above. They were collected at four different sites: Tiro Federal Sur, Portezuelo, La Viñita and R. Recalde, all within the Catamarca Valley (Fig. 1, a). Sample selection for further analyses followed pigment conservation criteria.

A set of 19 pottery sherds was studied (Tables 1 and 2). Figure 1(b) displays some of the samples analysed in which the colours characterized were white, black, reddish, dark brown, light brown, purple red or burgundy, and ochre. In order to ensure the PIXE results correspond only to the paint thickness, some of these samples were chosen for the characterization of the paste:

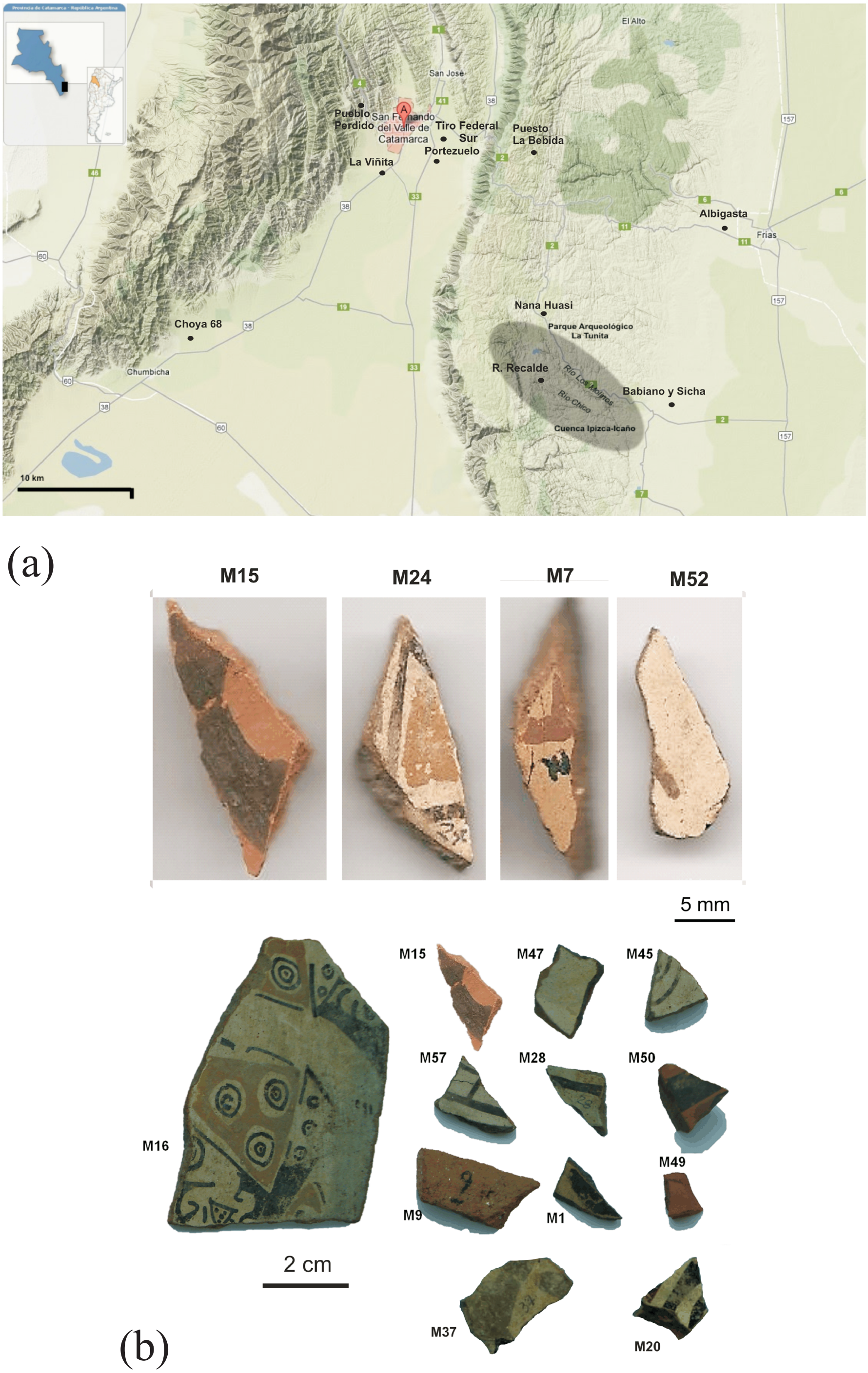

Figure 1 *(a) The Catamarca Valley and the archaeological sites; (b) representative decorated sherds chosen for the present analysis: M15, M24, M1, M50 (black); M7, M38 (reddish); M28, M47, M16, M57, M45, M24, M52 (white); M16, M24 (ochre); M9, M49, M15 and M7 (paste). [Colour figure can be viewed at wileyonlinelibrary.com]*

Table 1 *Main characteristics of the Aguada Portezuelo sherds*

Sample number	*Site*	*Ceramic form*	*Vessel form*	*Internal colour*	*External colour*	*Core colour*	*Texture*	*Firing*	*Surface treatment*	*Decoration*
M1	TSF	Globular	Lip/ neck	4/N black	2.5YR 5/6 red; 10YR 3/1 black; 2.5Y 8/2 white	6/N grey	Fine	Reduced	Smoothed-polished internal/external surface	Post-firing painting external surface
M2	TFS	Bowl	Body	4/N black	2.5Y 5/6 red; 7.5YR 6/6 brownish	6/N grey	Fine	Oxidized	Smoothed-polished internal/external surface	Pre-firing painting external surface graffited internal surface
M7	TFS	Globular vessel	Body	4/N black	2.5Y 8/1 white; 2.5YR 5/6 red	6/N grey	Fine	Reduced	Smoothed-polished internal/external surface	Post-firing painting external surface polished; graffited internal surface
M9	TFS	Globular vessel	Body	7.5YR 5/4 brownish	2.5Y 8/1 white	7.5YR 5/4 brownish	Coarse	Oxidized	Smoothed internal/external surface	Post-firing painting external surface
M13	Port	Vessel	Body	3/N black	2.5Y 3/1 black; 10R 4/3 red; 7.5YR 5/4 brownish; 2.5Y 8/1 white	4/N black	Fine	Reduced	Smoothed-polished internal/external surface	Pre- and post-firing painting internal/external surface
M15	Port	Vessel	Body	2.5Y 3/1 black; 7.5YR 5/4 brownish	7.5YR 5/4 brownish; 10R 4/3 red	7.5YR 5/4 brownish	Fine	Oxidized	Smoothed-polished internal/external surface	Pre- and post-firing painting internal/external surface
M16	Port	Globular vessel	Body	4/N black	2.5Y 3/1 black; 2.5Y 8/1 white; 7.5YR 6/6 yellow	6/N grey	Fine	Reduced	Smoothed-polished internal/external surface	Post-firing painting external surface/graffited internal surface

(*Continues*)

Table 1 *(Continued)*

Sample number	*Site*	*Ceramic form*	*Vessel form*	*Internal colour*	*External colour*	*Core colour*	*Texture*	*Firing*	*Surface treatment*	*Decoration*
M18	Port	Globular vessel	Body	4/N black	10R 4/3 red; 2.5YR 3/1 black; 2.5Y 8/1 white	6/N grey	Fine	Reduced	Smoothed-polished internal/external surface	Post-firing painting external surface graffited internal
M24	TFS	Globular vessel	Body	4/N black	2.5Y 8/1 white; 7.5YR5/4 brownish; 2.5Y 3/1 black	6/N grey	Fine	Reduced	Smoothed-polished internal/external surface	Post-firing painting external surface graffited internal
M28	LV	Vessel	Body	4/N black	2.5Y 3/1 black; 2.5Y 8/1 white; 7.5YR 5/4 brownish	6/N grey	Fine	Reduced	Smoothed-polished internal/external surface	Post-firing painting external surface graffited internal surface
M31	RR	Globular vessel	Body	4/N black	7.5 YR 5/4 brownish; 2.5Y 8/1 white	6/N grey	Fine	Reduced	Smoothed-polished internal/external surface	Post-firing painting external surface graffited internal surface
M37	TFS	Globular vessel	Body	7.5YR 5/4 brownish	2.5YR 5/6 red; 7.5YR 5/4 brownish	7.5YR 5/4 brownish	Fine	Oxidized	Smoothed-polished internal/external surface	Pre-firing painting external/internal surface
M45	Port	Globular vessel	Body	4/N black	2.5Y 3/1 black; 2.5Y 8/1 white	5/N grey	Fine	Reduced	Smoothed-polished internal/external surface	Post-firing painting external surface graffited internal surface
M47	Port	Globular vessel	Body	4/N black	2.5Y 8/1 white	6/N grey	Fine	Reduced	Smoothed-polished internal/external surface	Post-firing painting external surface graffited internal surface

(*Continues*)

Table 1 *(Continued)*

Sample number	*Site*	*Ceramic form*	*Vessel form*	*Internal colour*	*External colour*	*Core colour*	*Texture*	*Firing*	*Surface treatment*	*Decoration*
M49	Port	Globular vessel	Body	7.5YR 5/4 brownish	7.5YR 5/4 brownish	7.5YR 5/4 brownish	Fine	Oxidized	smoothed internal/external surface	Pre-firing painting external/internal surface
M50	Port	Bowl	Body	4/N black	2.5Y 3/1 black; 7.5YR 5/4 brownish	6/N grey	Fine	Reduced	Smoothed-polished internal/external surface	Post-firing painting external surface graffited internal surface
M52	Port	Vessel	Body	4/N black	2.5Y 8/1 white	6/N grey	Fine	Reduced	Smoothed-polished internal/external surface	Post-firing painting external surface graffited internal surface
M57	Port	Globular vessel	Body	4/N black	2.5Y 8/1 white	6/N grey	Fine	Reduced	Smoothed-polished internal/external surface	post-firing painting external surface graffited internal surface
MX	Port	Globular vessel	Body	4/N black	10R 4/3 red; 2.5Y 8/1 white	6/N grey	Fine	Reduced	Smoothed-polished internal/external surface	Post-firing painting external surface graffited internal surface
MX3	Port	Vessel	Body	7.5YR 5/4 brownish	7.5YR 5/4 brownish	7.5YR 5/4 brownish	Fine	Oxidized	Smoothed-polished internal/external surface	Post-firing painting external surface graffited internal surface

TFS: Tiro Federal Sur.

Table 2 *Particle-induced X-ray emission (PIXE) concentrations for major, minor and trace elements (n = 28)*

Sample	*Colour*	*Major (wt%)*									
		C	*O*	*Mg*	*Al*	*Si*	*K*	*Ca*	*Ti*	*Mn*	*Fe*
M1B	*Black*[1]	–	*33.7*	*1.3*	*4.38*	*11.1*	*3.6*	*6.38*	*0.7*	*27.7*	*8.96*
M50B	Black[1]	–	38	1.7	4.58	17	5.8	7.97	0.9	12.7	9.83
M18B	Black[1]	–	35.8	1.1	5.55	13.6	4	6.09	0.5	21	9.41
M24B	Black[2]	2.91	39.2	0.9	4.29	16.1	0.9	8.39	0.4	17.3	8.77
M15B	Black[2]	1.58	32.4	0.6	3.93	12.9	1.4	0.05	0.3	16.4	29.1
M2Br	Burgundy[1]	–	41.1	1.3	9.24	18.8	10	2.79	1.6	0.24	13.4
M15Br	Burgundy[1]	–	38.2	1.2	4.5	14.5	5	4.02	0.6	0.14	30.4
M18Br	Burgundy[1]	–	36.7	0.9	4.41	13.6	7	3.3	0.8	0.2	27.7
M28DB	Dark brown[1]	–	33.8	0.9	2.7	7.95	2.2	10.7	0.3	8.33	31.9
M31LB	Light brown[1]	–	39.3	2.7	8.37	15.5	9.3	4.68	1.6	3.04	14.5
M38R	Reddish[1]	–	40.1	0.9	8.28	16.8	7.4	4.01	1.2	0.39	20.2
MXR	Reddish[1]	–	39.9	0.8	8.32	16.5	8	6.65	1.1	0.16	17.9
M7R	Reddish[2]	3.32	41	0.6	4.72	25.3	4.8	1.07	0.4	0.15	17.3
M13W	White[1]	–	41.3	1.1	8.25	19.4	6.3	14.1	1	0.07	7.1
M28W	White[1]	–	38	0.8	5.87	14.1	5.3	25.5	0.9	1.03	7.75
M47W	White[1]	–	39.1	1.6	7.29	14.6	2.6	26.3	0.9	0.22	6.47
M57W	White[1]	–	38.8	2.2	6.38	14.2	2.4	25	1.1	1.34	6.35
M16W	White[1]	–	35.2	1.3	3.23	9.7	3.1	42.3	0.6	0.15	2.97
M45W	White[1]	–	39.2	2.5	6.86	14.8	2.7	26.9	0.9	0.16	3.62
M24W	White[2]	6.32	43.4	1	7.94	20.4	1.8	14.7	0.4	0.16	2.81
M52W	White[2]	1.65	41.2	1.5	10	21.2	1.7	15.8	0.6	0.09	3.47
M16O	Ochre[1]	–	42.9	1	7.13	23	6.9	8.47	1	0.18	8.21
M24O	Ochre[2]	6.27	45.4	0.9	5.81	26.1	3.2	7.11	0.4	0.04	3.62
M9P	Paste[1]	–	43.6	1.7	8.35	23.4	7.2	3.54	1.3	0.3	9.27
M49P	Paste[1]	–	42.8	1.7	5.95	23	4.2	13.2	0.7	0.13	6.77
MX3P	Paste[1]	–	43.9	0.9	9.36	24.1	9.3	3.6	1.5	0.15	5.9
M7P	Paste[2]	2.42	41.4	1.4	11	24.6	7.6	3.11	0.8	0.12	5.79
M15P	Paste[2]	1.5	43.3	0.9	11.2	23.3	4.9	1.21	0.8	0.1	11.1

Sample	*Colour*	*Minor and traces* ($\mu g\,g^{-1}$)														
		Na	*P*	*S*	*Cl*	*Sc*	*V*	*Cr*	*Ni*	*Cu*	*Zn*	*Rb*	*Sr*	*Zr*	*Ba*	*Pb*
M1B	*Black*[1]	*6593*	*1775*	–	*973*	–	*1102*	–	–	*569*	*1075*	–	*641*	*197*	*9691*	–
M50B	Black[1]	5590	529	1041	994	–	826	–	–	261	381	–	1086	–	4764	–
M18B	Black[1]	14 683	–	2213	6547	–	1370	–	–	202	204	147	592	–	4575	–
M24B	Black[2]	3026	2536	418	1787	–	–	–	–	231	227	–	770	–	–	–
M15B	Black[2]	4438	772	655	665	94	670	80	112	591	281	–	–	–	5232	–
M2Br	Burgundy[1]	6869	569	427	343	–	232	172	–	4943	734	694	296	380	–	92
M15Br	Burgundy[1]	11 542	488	1967	617	–	–	78	–	182	160	–	350	–	–	–
M18Br	Burgundy[1]	36 518	–	974	15 690	–	–	149	–	694	579	–	209	–	–	–
M28DB	Dark brown[1]	3101	2843	980	232	–	481	–	–	211	–	–	724	–	4545	–
M31LB	Light brown[1]	5917	847	700	768	–	–	152	263	201	357	116	300	351	–	–
M38R	Reddish[1]	4503	402	500	2337	–	–	131	–	154	94	181	285	143	–	–
MXR	Reddish[1]	4640	1445	353	324	–	–	128	–	114	525	177	135	258	–	–
M7R	Reddish[2]	10 246	1725	1102	384	–	–	82	152	–	312	–	–	–	–	–
M13W	White[1]	7222	1366	378	1771	–	–	152	–	1838	450	–	348	–	–	225
M28W	White[1]	3204	2804	1375	879	–	–	–	–	32	88	–	–	609	–	–
M47W	White[1]	3034	2313	465	1704	–	–	110	–	302	297	–	568	–	–	294
M57W	White[1]	8562	2830	2803	1518	–	–	179	–	496	966	208	1007	539	2505	543
M16W	White[1]	4155	2138	4309	2433	–	–	137	–	166	127	–	604	–	–	163
M45W	White[1]	14 918	2297	849	3129	–	149	–	–	128	510	–	476	–	–	133
M24W	White[2]	4446	3374	723	2260	1081	–	34	–	143	–	102	–	–	–	–
M52W	White[2]	18 503	6852	126	1099	701	–	376	–	70	653	–	–	–	–	–
M16O	Ochre[1]	7825	2115	782	443	–	–	107	50	215	248	351	395	–	–	41
M24O	Ochre[2]	5596	3711	1013	605	–	–	59	45	26	157	111	223	242	–	–
M9P	Paste[1]	7937	1062	410	2389	–	–	95	47	91	255	202	362	596	–	–
M49P	Paste[1]	12 057	680	690	622	–	121	–	86	–	171	134	460	–	–	–
MX3P	Paste[1]	8126	1421	590	1346	–	–	205	147	–	420	244	403	174	–	269
M7P	Paste[2]	15 400	1178	1251	375	–	–	158	197	50	275	–	–	–	–	–
M15P	Paste[2]	12 127	784	1385	1381	78	178	105	170	78	158	–	–	–	–	–

[1] Measurementes done at UFRGS with Be detector window.

[2] Measurements done at CAB with SDD detector polymer ultra-thin window.

M49, M7, M15, MX3 (fine texture) and M9 (coarse texture). All these pieces bear approximate dimensions of 1.5 × 1 cm, excepting sample M16 (4 × 4 cm). Table 1 gives the information about the main characteristics of the sherds.

ANALYTICAL TECHNIQUES

Chemical and mineralogical characterizations were carried out using PIXE, SEM-EDS and XRD. The experimental conditions are detailed below, as well as the methodology followed for sample preparation and data processing in each case.

PIXE

Pottery sherds were analysed using a 2 MeV proton beam in two different tandem accelerators: an NEC 1.7 MV accelerator from Centro Atómico Bariloche (CAB, Argentina) and an NEC 3 MV accelerator from the Universidad Federal de Rio Grande do Sul (UFRGS, Brazil). The first has a high-counting rate SDD X-ray detector with an ultrathin polymer window, allowing the detection of energies ranging from 0.2 to 20 keV. The second has an Si (Li) conventional detector with a Be window, bearing a better efficiency for high energy lines, that is, from 1 to 26 keV. In order to minimize radiation damage effects, low beam currents were used, around 0.5 nA. In all cases, the beam spot area at the sample surface was 1–9 mm^2.

PIXE spectra were processed with GUPIX software (GUPIXWIN v.2.2.4 Copyright © 2005, University of Guelph). For the spectra acquired at CAB, the analyses were performed as elemental quantifications, including O and C. For the spectra measured at UFRGS, oxygen characterization was carried out by stoichiometric association with the visible elements, through the most stable oxides; in these cases, it was not possible to quantify the carbon content. A statistical package developed at Missouri University Research Reactor (MURR) was used for the interpretation of the data. Statistical analysis was carried out on base-10 logarithms of the concentrations of all 25 chemical elements. The methods used to interpret compositional data obtained from the analysis of archaeological materials are discussed in detail elsewhere (e.g., Bishop and Neff 1989; Glascock 1992; Neff 2000, 2002) and will not be described in detail herein. Cluster and principal component analyses (PCAs) were performed for the PIXE data set. Groups were initially defined on the basis of the visual separation and further refined using group membership probabilities based on Mahalanobis distance projections (Bishop and Neff 1989).

XRD

XRD was used to characterize paints in pieces for which a reasonable amount of sample could be scraped from the surface. XRD patterns were recorded with a Philips X'Pert PRO PW3040/60 diffractometer, with Cu Kα X-ray radiation, Si monochromator, at 40 kV and 30 mA, step scan at 0.3° min^{-1} and step size of 0.02° 2θ. In all cases, only a small amount (a few milligrams) of material was available, so samples were mounted on an Si holder of low background.

SEM-EDS

SEM-EDS was carried out in a JEOL JXA 8230 equipment at the Laboratorio de Microscopía de Rayos X (LAMARX), National University of Córdoba, Argentina. Measurements were performed with an electron 15 keV electron beam and current of 9 nA. Samples were covered with Au in order to avoid the charge accumulation effect.

RESULTS AND DISCUSSION

PIXE

Figure 2 displays an example of the X-ray emission spectra obtained with each experimental set-up described above. The examples show the advantages and disadvantages of each detection system. The detector attached to the NEC 1.7 MV (ultrathin polymer window) allows the detection of light elements as C and O, although its efficiency rapidly decays for energies > 10 keV, which hinders the appropriate detection of elements such as Rb and Sr—although L emission could be registered, the detector resolution inhibits the adequate deconvolution from K-lines emitted by other major components (Si). On the other hand, the detector attached to the NEC 3 MV (beryllium window) is not well suited for the detection of elements with an atomic number < 10, but it exhibits a high efficiency for detecting characteristic energies > 10 keV.

Table 2 displays the quantification results after processing the spectra. In the reddish paints, different tones are present, which might be correlated with hematite (αFe_2O_3) content (Bertolino *et al*. 2009, Galvan Josa *et al.* 2010). This is observed in the Fe concentration with an average of 18.5% in samples M38, MX and M7 (range = 17.3–20.2%), whereas the more intense burgundy samples M2, M15 and M18 have a higher Fe content of around 23.8% on average (range =

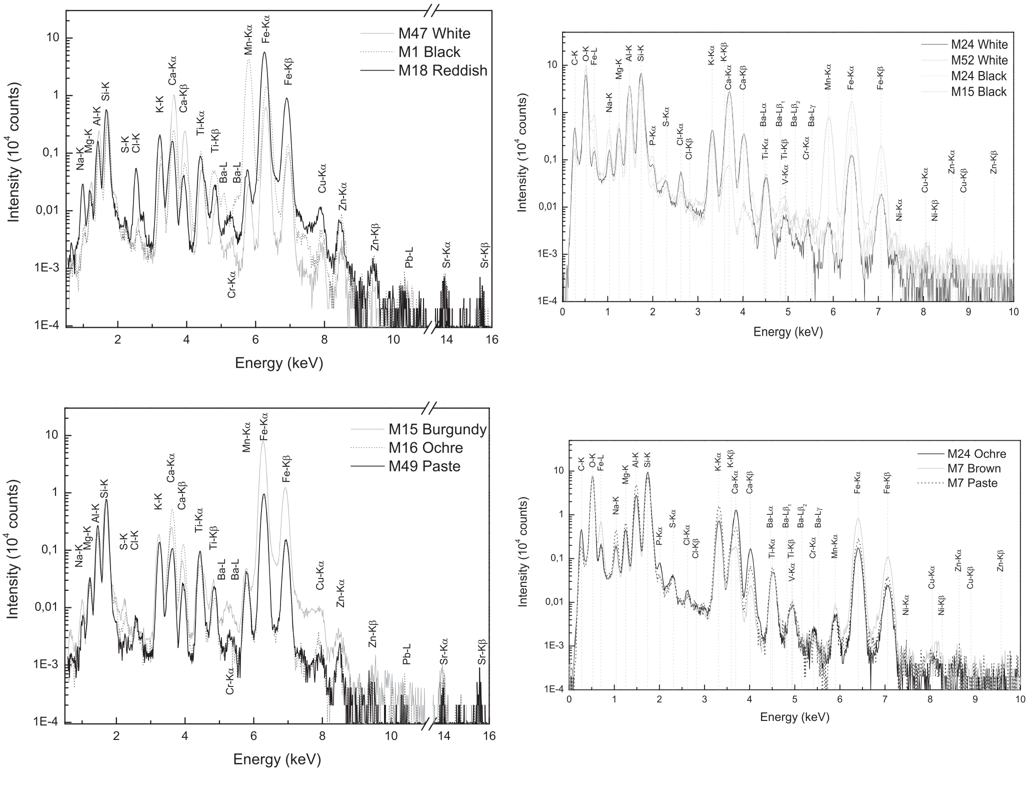

Figure 2 *Particle-induced X-ray emission (PIXE) spectra for 2 MeV for some of the white, black, reddish, ochre and brown paints. Measurements acquired in the NEC 3 MV (Universidad Federal de Rio Grande do Sul—UFRGS) (left) and at tandem 1.7 MeV (Centro Atómico Bariloche—CAB) (right). The elements determined are also shown.*

13.42–30.44%). Brown paint samples such as M28 also have a high Fe content (31.88%), but, unlike the reddish paints, a higher Mn concentration is present (8.33%). Light brown regions (M31) were painted over a white base and present lower concentrations for Fe (14.51%) and Mn (3.04%) than sample M28. A careful examination of the coloured region of this sample showed a deteriorated and non-homogeneous spoiled surface; thus, the beam could have also reached the substrate of the coloured region (paste), which is reflected in the higher Al (8.37%) and Si (15.47%) contents. Regarding the ochre paints, the composition obtained was very dissimilar, with variable Fe content ranging from 3.62% (M24) to 8.21% (M16). Also, great differences are observed in transition metals such as Cr, Cu and Zn. The composition of this paint is similar to that of the paste (mainly high concentration of Si associated to glass and quartz), though richer in Ca.

Concerning the trace elements, it is important to observe that Ba was detected in four out of five black post-firing paintings analysed. Additionally, it seems that the amount of Ba is positively correlated to the Mn concentration. This suggests that the black colour precursor might be psilomelane mineral group ($BaMn^{2+}(Mn^{4+})_8O_{16}(OH)_4$), a hydrous manganese oxide with variable amounts of Ba and P. Psilomelane group includes hollandite and romanechite minerals. Psilomelane sometimes is present with vanadinite intergrowth crystals, which perhaps could explain the V/Ba positive correlation observed in the PIXE results. V also occurs associated with barite, a barium sulfate ($BaSO_4$), although the lack of Pb in these samples makes it difficult to explain this correlation. In previous analytical research performed on Aguada Portezuelo paints, it was determined that the main identified mineral for this colour was pyrolusite (MnO_2), since Ba lines were not detected by EDS (De La Fuente *et al*. 2005).

The results obtained by PCA for major, minor and trace elements indicate that black, white and reddish-burgundy paintings might be divided into three groups, according to the Fe/Mn ratio, Ca content and the different Fe concentrations, respectively (Fig. 3, a, b). Figure 3(a) displays the PC1 and PC2 plot with the elements projections and the three groups defined by Mahlanobis distance; whereas Figure 3(b) shows the loading for the elements influencing each component. The first four principal components (PCs) explain 73.4% of the variance. Table 3 gives the chemical information for each defined group.

Group 1, the black paintings, presents variable concentrations of Fe and Mn, and in some cases they positively correlate (Fig. 3, a). They can be divided in three subgroups according to the Fe/Mn ratio: subgroup A, Fe/Mn: 0.515 (M18, M24) with 19.12% Mn and 9.09% Fe average; subgroup B, Fe/Mn: 0.47 (M50, M28) with 10.52% Mn and 20.85% Fe average; and subgroup C, Fe/Mn: 0.32 (M1) with 27.69% Mn and 8.96% Fe (Fig. 3, c, and Table 2). One sample, M15, is definitely an outlier, with a Fe/Mn: 1.78 (16.35% Mn and 29.14% Fe). This variation in the ratio of Fe/Mn is also expressed in Raman analysis with the alternative presence of Mn oxide minerals and hematite compounds (De La Fuente and Pérez Martínez 2008, 2018).

Group 2 shows the white paintings. Here, three subgroups were found: subgroup A (M57, M28), with an average of 25.22% Ca; subgroup B (M47, M45, M24, M16), with an average of 27.22% Ca; and subgroup C (M52), with a Ca concentration of 15.78% (Fig. 3, c). Sample M13 is an outlier with 14.12% Ca concentration. Some white paintings (subgroup B) exhibit different Pb in trace concentrations (ppt). In translucent media such as quartz, Pb might be the precursor of the white colour (Bertolino *et al*. 2009, Galvan Josa et al. 2010). Also, the presence of Pb in low concentrations in pre-firing paintings is sometimes indicative of its use as a fluxing agent to achieve an initial glazed-type ceramics (Van Keuren *et al*. 2013, Ferguson et al. 2017). Additionally, it is interesting to observe that one sample, M52, has an unusual amount

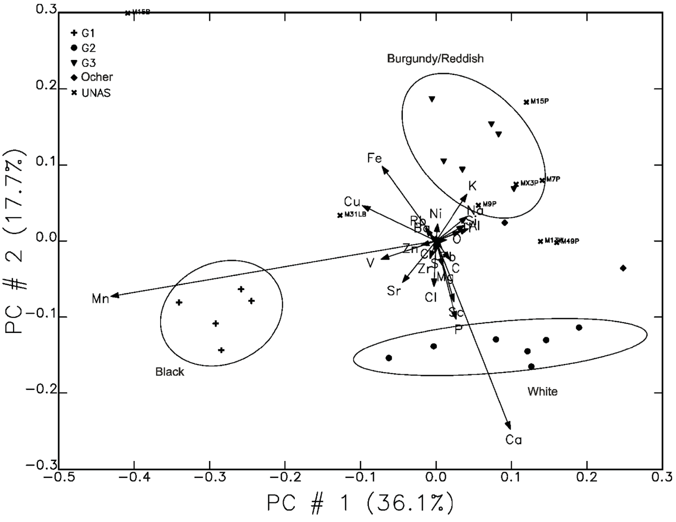

(a)

Loadings for the first 4 PC´s (n=28)

Variable	PC1	PC2	PC3	PC4
Mn	-0,9028	-0,2178	0,0984	-0,0130
Cl	-0,0059	-0,1792	-0,2398	-0,7702
Cu	-0,2047	0,1388	-0,7574	0,0909
Ca	0,2068	-0,7417	-0,1815	0,0699
S	-0,0017	-0,0459	0,1741	-0,4123
Zn	-0,0409	-0,0170	-0,3545	0,1649
P	0,0563	-0,3072	0,0811	0,1862
Na	0,0871	0,0964	-0,1153	-0,2861
Fe	-0,1499	0,2947	-0,0018	-0,0224
Sc	0,0503	-0,2390	-0,1017	0,1307
K	0,0859	0,1837	-0,1323	-0,0519
Ti	0,0684	0,0381	-0,2152	-0,0187
Rb	-0,0294	0,0492	-0,1571	0,1468
Sr	-0,0929	-0,1625	0,0159	-0,0281
V	-0,1524	-0,0719	0,0342	-0,0279
Cr	-0,0052	-0,0135	-0,1611	0,0520
Pb	0,0159	-0,0283	-0,0655	-0,1447
Mg	0,0182	-0,0985	-0,1048	-0,0257
Al	0,0900	0,0471	-0,0672	0,0373
Ni	0,0040	0,0671	-0,0585	-0,0819
Si	0,0802	0,0616	0,0307	0,0279
C	0,0379	-0,0728	0,0010	0,0090
Zr	-0,0171	-0,0684	0,0068	0,0401
Ba	-0,0172	0,0243	-0,0041	0,0318
O	0,0292	0,0045	0,0034	0,0100
Variance %	36,0865	17,7216	12,1626	7,4757

(b)

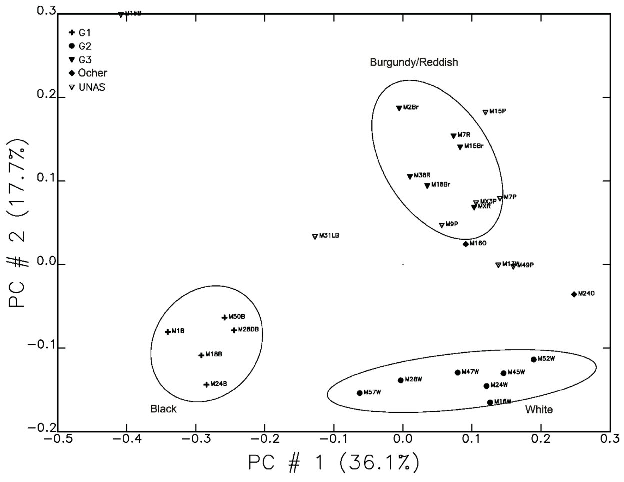

(c)

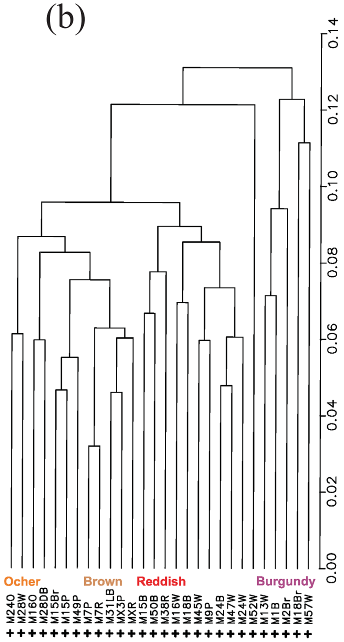

(d)

Figure 3 *(a) Principal component analysis (PCA) of major, minor and trace elements showing the discriminated colour groups (G1, black; G2, white; and G3, burgundy/reddish). UNAS, unassigned samples. Projected elements are also shown (ellipses represent 95% confidence). (b) Loadings for the first four principal components (PCs) (n = 28). (c) PC1 and PC2 showing groups 1–3, defined by Mahlanobis distances (ellipses represent 95% confidence). (d) Cluster analysis of minor and trace elements showing the discrimination of the red iron oxides-based pigments. [Colour figure can be viewed at wileyonlinelibrary.com]*

Table 3 *Element concentration and standard deviations (mean + SD) for the paintings compositional groups*

Element	*Group 1 (*n *= 5)*	*Group 2 (*n *= 7)*	*Group 3 (*n *= 9)*
C (%)	2.73 ± 0.39	3.06 ± 1.52	2.70 ± 0.44
O (%)	36.10 ± 2.47	39.25 ± 2.55	40.62 ± 2.31
Na	6598.6 ± 4779	8117.42 ± 6237	11 753.44 ± 9897
Mg (%)	1.15 ± 0.33	1.55 ± 0.61	1.07 ± 0.36
Al (%)	4.3 ± 1.02	6.79 ± 2.06	7.57 ± 2.41
Si (%)	13.15 ± 3.71	15.57 ± 3.97	19.71 ± 4.64
P	1841.81 ± 909	3229.71 ± 1652	1036.57 ± 465.22
S	984.29 ± 765	1521.42 ± 1504	841.56 ± 535
Cl	2106.6 ± 2545	1860.28 ± 793	2645 ± 4963
K (%)	3.27 ± 1.85	2.80 ± 1.20	7.36 ± 1.71
Ca (%)	7.90 ± 1.85	25.19 ± 9.08	3.57 ± 1.46
Sc	324.84 ± 54.11	480.60 ± 319	231.62 ± 76.50
Ti (%)	0.53 ± 0.24	0.77 ± 0.23	1.03 ± 0.41
V	845.18 ± 397	384.29 ± 153	376.02 ± 122.33
Cr	127.80 ± 41.18	154.34 ± 107.46	133.11 ± 42.84
Mn (%)	17.39 ± 7.46	0.45 ± 0.51	0.21 ± 0.09
Fe (%)	13.77 ± 10.13	4.77 ± 2.01	16.43 ± 8.83
Ni	94.29 ± 30.65	111.28 ± 34.47	121.89 ± 43.43
Cu	294.8 ± 154	191 ± 159.25	716.89 ± 1596.83
Zn	423.36 ± 370	423.78 ± 311	372.67 ± 208.72
Rb	199.91 ± 60.93	182.30 ± 50.49	232.45 ± 177.16
Sr	762.6 ± 193.66	580.49 ± 196	309.86 ± 89.28
Zr	324.56 ± 86.41	418.51 ± 131.35	298.45 ± 135.16
Ba	5637.50 ± 2267	4351.50 ± 993	4935.55 ± 607.56
Pb	174.65 ± 120	235.26 ± 148.13	198.06 ± 67.89

of P (6852 ppm), which could be indicative of the presence of hydroxyapatite (Table 2) (Cremonte *et al*. 2003).

On the other hand, PCA also clearly differentiates another group (group 3) involving mostly reddish and burgundy colour samples (Fig. 3, a). As contrarily thought, samples are discriminated in this group more as a function of the relative concentrations of transition metals (Cr, Ni, Cu, Zn) than following the Fe concentrations: subgroup A, samples M7 and M15, with an average of 23.84% Fe; subgroup B, samples M38 and M18, with an average of 23.93% Fe; and subgroup C, sample M2, with 13.42% Fe. A subgroup D, after projected samples for membership probabilities, is formed by samples MX, MX3 (paste), M7 (paste) and M9 (paste) with 7.64% Fe. One ochre sample, M16, is also plotted in the margin of this group (Fig. 3, c). Burgundy samples also present an unusual amount of Cu, Ni and Zn (ppm) in all the samples analysed, whereas ochre samples show higher Ca concentrations (Table 2). Therefore, it can be observed that different tonalities do not match with exact different chemical compositions, mainly of Fe concentration. The presence of Fe as different Fe oxides (such as hematite) gives the red colour for these paintings (mostly post-firing), although the chemical variations observed are due mainly to the presence of different concentrations of trace elements such as Cu, Zn, Ba and Zr. Different tonalities in post-firing paintings are due to different recipes used by ancient potters involving different mixed minerals as colorants. The subgroups observed for the red Fe-based paintings are related to the origin of raw materials used by potters.

A further exploration using only minor and trace elements was carried out by cluster analysis (Fig. 3, d). Results show higher variations between samples of the same colour (e.g., white and black), although for burgundy/reddish/ochre/brown samples the plot shows a good discrimination based on Euclidean distances. Trace elements responsible for this discrimination are Cr, Cu, Zn, and Zr. These preliminary results could indicate that several geochemically different sources of raw materials were introduced to produce these red Fe-based pigments, mainly reddish, burgundy, brown and ochre.

XRD

XRD was applied to white pre-firing slips, and ochre and reddish post-firing paints (Fig. 4, a). Also, some paste analyses were carried out. In all cases, the extracted materials also contained some grains from the underlying pastes, which is reflected in the bulk mineralogy by presence of quartz, feldspars, micas, amphibole and hematite. As shown in Figure 4(a), white paints are characterized by Ca-bearing minerals such as ghelenite, calcite and gypsum (cf. De La Fuente and Pérez Martínez 2008, 2018). In some cases, both the low intensity of reflections of micas and feldspars, and the presence of new higher temperature mineral phases (hematite and ghelenite) were observed. Ghelenite is an aluminosilicate that forms from mixtures of calcite with clay minerals (paste) at between 850–900 and 1050°C, and beyond that temperature it forms anorthite. This indicates that the firing temperature may have reached or exceeded 900–1000°C, as previously reported (Bertolino *et al.* 2009). Ghelenite and CaO in ceramic pastes could be an indication of the presence of calcite in the original raw material, and it could act as a flux to decrease the required firing temperature, also contributing to the vitrification and the formation of vesicles to liberate CO_2. As pointed out by Bertolino et al. (2009, 97, fig. 4), if dissociation of calcite were not completed (approximately 750–850°C), the sequence of gehelenite, calcite and CaO may coexist in the range 700–900°C. The absence of gehelenite might be an indication of lower firing temperatures around 900°C (Bertolino *et al.* 2009, 98). Gypsum has been reported as being used as a decorative white pigment (Palamarczuk *et al.* 2007; Centeno *et al.* 2012; Freire *et al.* 2018). The presence of gypsum as pre-firing white paint in one sample (M16) is difficult to explain (Figs 1 and 4, a). This sample has the highest Ca (42.3 wt%) and S (4309 ppm) concentrations among the white samples (Table 2). Gypsum is a calcium sulfate dehydrate mineral ($CaSO_4.2H_2O$) and is both available in nature from chemical sedimentary rock formations or generally culturally produced through a calcining technology using limestone rocks (*aljez*) (Harrell 2014, 2017). The impure form of gypsum is called gypsite; it is present in some natural soil formations. Bassanite ($CaSO_4.1/2H_2O$, calcium sulfate hemihydrate) and anhydrite ($CaSO_4$, anhydrous calcium sulfate) are other forms of calcium sulfates; they are subsequently obtained by dehydration of the original gypsum by heating (Harrell 2017, 537). The presence of gypsum as a slip in the vessels (perhaps mixed with clay) implies that its application on the ceramic surface by potters was in a post-firing context, since its physical and chemical properties change through subsequent higher temperatures giving different forms of anhydrite, or 'dead gypsum' (Villanueva Dominguéz and García Santos 2001). It is not yet clear if the gypsum were obtained by heating the *aljez* or from gypsite deposits, although the evidence of use of gypsum in rock art in the area, and the discovering of a natural gypsum source, points to the use of this source in pre-Hispanic times (Nazar and De La Fuente 2016). Finally, the ochre and reddish post-firing paintings analysed in this work are characterized by hematite (Fig. 4, a) (De La Fuente and Pérez Martínez 2008, 2018; Bertolino *et al.* 2009).

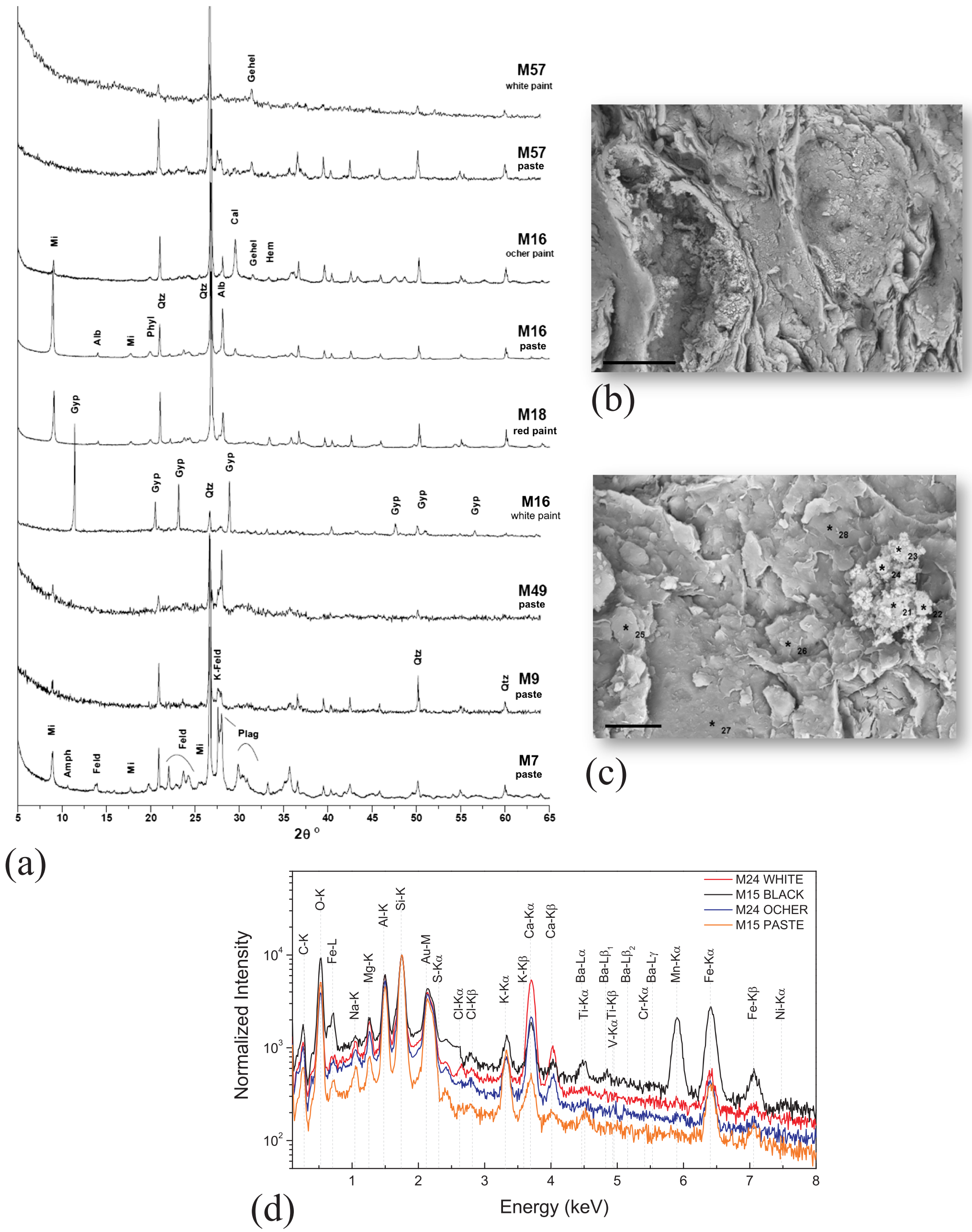

Figure 4 *(a) X-ray diffraction (XRD) spectra for white pre-firing slip, ochre and reddish post-firing paints. Some paste samples are also shown. (b) Scanning electron microscopy (SEM) secondary electron images for M15 sample showing vitrified textures. (c) Neoformation mineral phases. (d) Electro Probe Micro-Analizer (EPMA) spectra for M15 (black), M24 (white), M24 (ochre) and M15 (paste). [Colour figure can be viewed at wileyonlinelibrary.com]*

SEM-EDS

The paste analysis by SEM allows the observation and identification of materials almost completely melted, characterized by vitreous textures with an important bubble and tubule abundance created by escaping gases during the paste melting process (Fig. 4, b). Within pores, very fine grained materials can be distinguished, composed of Ca, Fe or Si (Fig. 4, c). These can be interpreted as new phases produced by the reaction of mineral components at high temperatures (Bertolino *et al.* 2009, Galvan Josa *et al.* 2010).

Irregular and very fine particle aggregates, eventually < 200 nm in the vesicle walls or forming part of the matrix, have been observed (Fig. 4, c). They have a highly variable composition, but always bearing high O concentration (probably oxides), contrasting with the paste compositions. EDS analyses on white, black and ochre paintings show very similar results to those obtained by PIXE (Fig. 4, d, and Table 2). In all the samples, white paint has a high Ca content; the black one, Fe and Mn plus minor Ca (Fig. 4, d). Ochre paint shows a medium to high Fe concentrations, and also Ca from the substratum. All the paints have an alumino-silicate composition ($Al + Si$) evidencing the existence of a clayish vehicle to transport the colourant pigment (Fig. 4, d) in accordance with previous SEM-EDS research performed on this pottery (De La Fuente *et al.* 2005; see also De La Fuente and Pérez Martínez 2008, 181, fig. 10). It is unknown if a flux or binder has been added to the $Al + Si + \text{pigment}$ system before (for the white slip) and/or after (for reddish, burgundy, ochre and black paintings) the firing, although the examination of hundreds of sherds of Aguada Portezuelo pottery shows for the post-firing colours an unusual amount of pigment applied on the surface of the vessels, suggesting the possibility of some kind of binder applied to fix the pigment into the porous ceramic surface.

CONCLUSIONS

Multi-elemental PIXE chemical results, in combination with a robust PCA statistical treatment of data, allowed the examination of the compositional ranges of various pre- and post-firing paintings on Aguada Portezuelo pottery. Nowadays, the main advantage of PIXE is its almost non-destructive nature, and the possibility to obtain concentrations of ppm and even ppt for certain specific elements. In the present study, different painting colour groups (black, white and burgundy/reddish) could be rapidly discriminated by PIXE. Particularly in black paintings, the presence of different Fe/Mn ratios with the presence of Ba suggests the use of a psilomelane group mineral as an inorganic mineral precursor for the post-firing black paintings. Mn oxide-based minerals are often chemically complex. The psilomelane group involves at least two oxides: hollandite and romanchite, and it has an amorphous nature containing admixed impurities such as Fe hydroxides. Thus, it is easily processed by potters as a pigment. White pre-firing slips are chemically characterized by Ca expressed in different concentrations, although through XRD different Ca-bearing metastable mineral phases such as calcite, gehlenite and gypsum were identified. Interestingly, one white sample determined by PIXE showed an unusual P concentration, suggesting the possibility of hydroxyapatite presence in the pre-firing slip. Burgundy, reddish and ochre post-firing paintings are clearly characterized by Fe, where α hematite was the main pigment used by ancient potters. Trace element analysis did not produce direct correlations between paint colour and chemical compositions, probably mainly due to the different recipes applied by potters. However, trace elements discriminated fairly well these tonalities, suggesting the use of different geochemical sources of raw materials for the pigments. Definitely, PIXE studies have much to do in future for the identification of different Fe oxides pigment sources used by ancient potters, especially by using minor and trace elements (David et al. 1993; Erlandson *et al*. 1999, Lebon *et al*. 2018). Comparatively with vibrational techniques such as Raman microspectroscopy, PIXE allows one to explore the compositional chemical concentrations of the main pigments involved in the decoration of the vessels, thus complementing the information achieved through other analytical techniques. Finally, SEM-EDS studies contributed to a better understanding of the changes overcome, through different firing temperatures, in the physical and chemical structures of the ceramic matrixes.

ACKNOWLEDGEMENTS

This research was fully funded by the National Research Scientific Council (CONICET), Argentina. V. G. and S. L. acknowledge CONICET for partial funding through different postdoctoral fellowships to develop the PIXE analyses. The Direction of Anthropology, Government of Province of Catamarca, provided permission to analyse the samples within the project 'Cadenas Operativas y Elecciones Tecnológicas en la Producción de Alfarería Arqueológica y Pinturas Rupestres durante el Período Agroalfarero Medio (ca. AD 600–AD 900) en la Cuenca Ipizca-Icaño (Dptos. Ancasti y La Paz, Catamarca, Argentina): Una Aproximación Arqueométrica'.

REFERENCES

Abd El Aal, S., Korman, A., Stonert, A., Munnik, F., and Turos, A., 2009, Ion beam analysis of ancient Egyptian wall paintings, *Vacuum*, **83**, S4–S8.

Baldini, M., Carbonari, J., Cieza, G., de Feo, M., del Castillo, M., Figini, A., Rex González, A., Huarte, R., and Togo, J., 2002, Primer análisis de la cronología obtenida en el sitio Choya 68 (Depto. de Capayán, Provincia de Catamarca, Argentina), *Estudios Atacameños*, **24**, 71–82.

Bertolino, S. R., Galván, V., Carreras, A., Laguens, A., De La Fuente, G., and Riveros, A., 2009, X-ray techniques applied to surface paintings of ceramic pottery pieces from Aguada culture (Catamarca, Argentina), *X-Ray Spectrometry*, **38**, 95–102.

Bishop, R. L., and Neff, H., 1989, Compositional data analysis in archaeology, in *Archaeological chemistry I. advances in chemistry*Series 220 (ed. R. O. Allen), 57–86, American Chemical Society, Washington, D. C.

Calligaro, T., González, V., and Pichon, L., 2015, PIXE analysis of historical paintings: Is the gain worth the risk? *Nuclear Instruments and Methods in Physics Research B*, **363**, 135–43.

Centeno, S., Williams, V., Little, N., and Speakman, J., 2012, Characterization of surface decorations in Prehispanic archaeological ceramics by Raman spectroscopy, FTIR, XRD and XRF, *Vibrational Spectroscopy*, **58**, 119–24.

Cremonte, M. B., Baldini, M., and Botto, I. L., 2003, Pastas y colores, Un camino al conocimiento del estilo Portezuelo de Aguada, *Intersecciones en Antropología*, **4**, 3–16.

Dasari, K. B., Acharya, R., Ray, D. K., and Lakshmana Das, N., 2017, Application of PIXE for the determination of transition elements in the grouping study of archaeological clay potteries, *X-Ray Spectrometry*, **46**, 180–5.

David, B., Clayton, E., and Watchman, A., 1993, Initial results of PIXE analysis on northwestern Australian ochers, *Australian Archaeology*, **36**, 50–7.

De La Fuente, G. A., and Pérez Martínez, J. M., 2008, Estudiando pinturas en cerámicas arqueológicas 'Aguada Portezuelo' (ca. 600–900 AD) del Noroeste Argentino: nuevos aportes a través de una aproximación arqueométrica por microespectroscopía de Ramán (MSR), *Intersecciones en Antropología*, **9**, 173–86.

De La Fuente, G. A., and Pérez Martínez, J. M., 2018, Ancient potters, paintings and craft specialization in northwestern argentine region: New data through Raman characterization of pre- and postfiring ceramic paintings on Aguada Portezuelo ceramics from middle period (Catamarca, Argentina), *Archaeological and Anthropological Sciences*, https://doi.org/10.1007/s12520-018-0676-9.

De La Fuente, G. A., Kristcautzky, N., Toselli, G. A., and Riveros, A., 2005, Petrología cerámica comparativa y análisis composicional de las pinturas por MEB-EDS de estilo Aguada Portezuelo (ca. 600–900 DC) en el Valle de Catamarca (Noroeste Argentino), *Estudios Atacameños*, (30), 61–78.

Erlandson, J. M., Robertson, J. D., and Descantes, C., 1999, Geochemical analysis of eight red ochres from western North America, *American Antiquity*, **64**, 517–26.

Ferguson, J. R., Van Keuren, S., and Bender, S., 2017, Rapid qualitative compositional analysis of ceramic paints, *Journal of Archaeological Science: Reports*, **3**, 321–7.

Freire, E., Halac, E. B., Polla, G., Reinoso, M., Basile, M., and Ratto, N., 2018, Análisis de rellenos en surcos incisos y excisos en pucos de Fiambalá (Catamarca, Argentina), *Intersecciones en Antropología*, **19**, 17–24.

Gajić-Kvaščev, M., Stojanović, M. M., Šmit, Ž., Kantarelou, V., Karydas, A. G., Šljivar, D., Milovanović, D., and Andrić, V., 2012, New evidence for the use of cinnabar as colouring pigment in the Vinča culture, *Journal of Archaeological Science*, **39**, 1025–33.

Galván Josa, V., Bertolino, S., Laguens, A., Riveros, J., and Castellano, G., 2010, X-ray and Scanning Electron Microscopy archaemetric studies of pigments from the Aguada Culture, Argentina, *Microchemical Journal*, **96**, 259–68.

Galván Josa, V., Bertolino, S. A., Riveros, J., and Castellano, G., 2009, Methodology for processing backscattered electron images. Application to Aguada archaeological paints, *Micron*, **40**, 793–9.

Glascock, M. D., 1992, Characterization of archaeological ceramics at MURR by neutron activation analysis and multivariate statistics, in *Chemical characterization of ceramic pastes in archaeology* (ed. H. Neff), 11–26, Prehistory Press, Madison, WI.

González, A., 1998, *Arte precolombino: Cultura la Aguada. Arqueología y sus diseños*, Filme Ediciones, Valero.

Grassi, N., Bonanni, P., Mazzotta, C., Migliori, A., and Mandò, P. A., 2009, PIXE analsysis of a painting by Giorgio Vasari, *X-Ray Spectrometry*, **38**, 301–7.

Hall, B., 2006, *PIXE analysis of oil-paint pigments: proof of principle*. Bachelor of science thesis. Department of Physics and Astronomy, Brigham Young University.

Harrell, J. A., 2014, Report of geological prospection in the vicinity of Amarna, *Journal of Egyptian Archaeology*, **100**, 25–33.

Harrell, J. A., 2017, Amarna gypsite: A new source of gypsum for ancient Egypt, *Journal of Archaeological Science: Reports*, **11**, 536–45.

Ikeoka, R.A., Appoloni, C.R., Rizzutto, M.A., Silva T.F., & Bandeira, A.M., 2013, PIXE analysis of pre-colonial pottery from Sambaqui do Panaquatira, *13th PIXE conference*,

Kusch, M. F., 1996–97, Estructura y diseño en la cerámica Portezuelo, *Shincal*, **6**, 241–8.

Laguens, A., 2007, Contextos materiales de desigualdad socialen el valle de Ambato, Catamarca, Argentina,entre los siglos VII y X d.C, *Revista Española de Antropología Americana*, **37**, 27–49.

Lebon, M., Pichon, L., and Beck, L., 2018, Enhanced identification of trace element fingerprint of prehistoric pigments by PIXE mapping, *Nuclear Instruments and Methods in Physics Research Section B*, **417**, 91–5.

Lima, S. C., Rizzutto, M. A., Added, N., Barbosa, M. D. L., Trindade, G. F., and Fleming, M. I. D. A., 2011, Pre-Hispanic ceramics analyzed using PIXE and radiographic techniques, *Nuclear Instruments and Methods in Physics Research B*, **269**, 3025–31.

Nazar, D. C., and De La Fuente, G. A., 2016, Acerca de la cerámica Aguada Portezuelo del Valle de Catamarca y la sierra de Ancasti, *Comechingonia*, **20**, 153–88.

Neelmeijer, C., Brissaud, I., Calligaro, T., Demortier, G., Hautojärvi, A., Mäder, M., Martinot, L., Schreiner, M., Tuurnala, T., and Weber, G., 2000, Paintings—a challenge for XRF and PIXE analysis, *X-Ray Spectrometry*, **29**, 101–10.

Neff, H., 2000, Neutron activation analysis for provenance determination in archaeology, in *Modern analytical methods in art and archaeology* (eds. E. Ciliberto and G. Spoto), 81–134, John Wiley and Sons, Inc., New York.

Neff, H., 2002, Quantitative techniques for analyzing ceramic compositional data, in *Ceramic source determination in the greater southwest* (eds. D. M. Glowacki and H. Neff), Monograph *44*, Cotsen Institute of Archaeology, UCLA, Los Angeles.

Olsson, A.-M. B., Calligaro, T., Colinart, S., Dran, J. C., Lövestam, N. E. G., Moignard, B., and Salomon, J., 2001, Micro-PIXE analysis of an ancient Egyptian papyrus: Identification of pigments used for the 'book of the dead', *Nuclear Instruments and Methods in Physics Research B*, **181**, 707–14.

Palamarczuk, V., Fernández de Rapp, M. E., and Lascalea, G. E., 2007, Aproximaciones a la caracterización del material Blanco decorativo de la cerámica Famabalasto negro Grabado, in *Cerámicas Arqueológicas: Perspectivas Arqueométricas Para su Análisis e Interpretación* (eds. M. B. Cremonte and N. Ratto), 27–37, Editorial de la Universidad Nacional de Jujuy, Jujuy, Argentina.

Pantorrilla, M., and Núñez Regueiro, V., 2006, Investigaciones arqueológicas en la zona de Escaba, provincia de Tucumán: Asentamientos Condorhuasi y Aguada en las Yungas, *Intersecciones en Antropología*, **7**, 235–45.

Pappalardo, L., La Rosa, V., Rizzo, F., and Romano, F. P., 2015, Non-destructive PIXE-alpha characterisation of pigments in Kamares pottery (1850–1700 BC) from Phaistos (Crete), *X-Ray Spectrometry*, **44**, 276–81.

Pappalardo, L., Barresi, S., Biondi, G., Caliri, C., Caruso, F., Catalano, R., Lamagna, G., Manenti, G. A., Monterosso, G., Orlando, A., Rizzo, F., Romano, F. P., and Santos, H. C., 2016, PIXE-alpha non-destructive and *in situ* compositional investigation of black gloss on ancient pottery, *X-Ray Spectrometry*, **45**, 258–62.

Pérez Gollán, J., 1991, La Cultura de la Aguada vista desde el Valle de Ambato, *Publicaciones Arqueología CIFFyH* Córdoba, **46**, 157–74.

Poupeau, G., Le Bourdonnec, F.-X., Carter, T., Delerue, S., Shackley, M. S., Barrat, J.-A., Dubernet, S., Moretto, P., Calligaro, T., Milić, M., and Kobayashi, K., 2010, The use of SEM-EDS, PIXE and EDXRF for obsidian provenance studies in the near east: A case study from Neolithic Çatalhöyük (Central Anatolia), *Journal of Archaeological Science*, **37**, 2705–20.

Rivero-Torres, S., Calligaro, T., Tenorio, D., and Jiménez-Reyes, M., 2008, Characterization of archaeological obsidians from Lagartero, Chiapas Mexico by PIXE, *Journal of Archaeological Science*, **35**, 3168–71.

Rizzuto, A. M., and Tabacniks, M. H., 2017, Particle induced X-ray Emssion (PIXE) and its application in ceramic analysis, in *The Oxford handbook of archaeological ceramic analysis* (ed. A. Hunt), 23–54, Oxford Handbooks Online, Oxford, UK.

Rizzuto, A. M., Tabacniks, M. H., Added, N., Barbosa, M. D. L., Curado, J. F., Pascholatt, P. R., Neves, G., Lima, S. C., and Melo, H. G., 2007, Pixe Externo Para Análises de Objetos de Arte e Arqueologia, *Revista Brasileira de Arqueometria, Restauração e Conservação*, **1**, 309–12.

Rizzutto, M. A., Moro, M. V., Silva, T. F., Trindade, G. F., Added, N., Tabacniks, M. H., Kajiya, E. M., Campos, P. H. V., Magalh£es, A. G., and Barbosa, M., 2014, External-PIXE analysis for the study of pigments from a painting from the Museum of Contemporary art, *Nuclear Instruments and Methods in Physics Research B*, **332**, 411–14.

Roumié, M., Wicenciak, U., Bakraji, E., and Nsouli, B., 2010, PIXE characterization of Lebanese excavated amphorae from Jiyeh archeological site, *Nuclear Instruments and Methods in Physics Research Section B: Beam Interactions with Materials and Atoms*, **268**, 87–91.

Ruvalcaba-Sil, J. L., 2005, PIXE analysis of pre-Hispanic items from ancient America, in *X-rays for archaeology* (eds. M. Uda, G. Demortier, and I. Nakai), 123–49, Springer, Dordrecht.

Ruvalcaba-Sil, J. L., and Demortier, G., 1997, Scanning RBS-PIXE study of ancient artifacts from South America using microbeam, *Nuclear Instruments and Methods in Physics Research B*, **130**, 297–302.

Ruvalcaba-Sil, J. L., Ontalba Salamanca, M. A., Manzanilla, L., Miranda, J., Cañetas Ortega, J., and López, C., 1999, Characterization of pre-Hispanic pottery from Teotihuacan, Mexico, by a combined PIXE-RBS and XRD analysis, *Nuclear Instruments and Methods in Physics Research B*, **150**, 591–6.

Santos, H. C., Added, N., Silva, T. F., and Rodrigues, C. L., 2015, External-RBS, PIXE and NRA analysis for ancient swords, *Nuclear Instruments and Methods in Physics Research B*, **345**, 42–7.

Šmit, Ž., Milavec, T., Fajfar, H., Rehren, T., Lankton, J. W., and Gratuze, B., 2013, Analysis of glass from the post-Roman settlement Tonovcov grad (Slovenia) by PIXE–PIGE and LA-ICP-MS, *Nuclear Instruments and Methods in Physics Research B*, **311**, 53–9.

Van Keuren, S., Neff, H., and Agostini, M. R., 2013, Glaze-paints, technological knowledge and ceramic specialization in the fourtheenth-century Pueblo southwest, *Journal of Anthropological Archaeology*, **32**, 675–90.

Villanueva Dominguéz, L., and García Santos, A., 2001, *Manual del Yeso*, Asociación Técnica y Empresarial del Yeso, S. L. CIE Inversiones Editoriales Dossat. Madrid.